Fine Extraction of Water Boundaries Based on an Improved Subpixel Mapping Algorithm

NA ZHANG[ID], PING WANG[ID], AND XIN ZHAO

College of Geodesy and Geomatics, Shandong University of Science and Technology, Qingdao 266590, China

Corresponding author: Ping Wang (1043222145@qq.com)

ABSTRACT The fine extraction of water boundaries is of great significance for water resource monitoring, water environment monitoring, and flood prevention. MODIS images are widely used for water extraction due to their high temporal resolution, wide coverage, gratuity, and long observation period. However, owing to their low spatial resolution, the water boundary results are often blurred. It is difficult to extract water boundaries accurately. The subpixel mapping algorithm can solve this problem. In this article, Dongting Lake and its surroundings are adopted as the experimental area. The digital elevation model (DEM) is used to modify the subpixel/pixel spatial attraction model (SPSAM) mapping results. The proposed algorithm is referred to as the DEM-modified SPSAM (D-MSPSAM). Based on the visual results of the two sets of experiments, the modified results suitably maintain the spatial details of the water, and many of the underestimations caused by the similarity of the spectral characteristics of the surroundings to those of the water have been corrected. In this paper, the accuracy of Landsat-8 water extraction is used as a reference. Based on the quantitative results, the D-MSPSAM method has a higher extraction accuracy than the traditional threshold method, and the accuracies of the extraction for high water and low water have been increased by 3.56 percentage points and 2.77 percentage points, respectively. Furthermore, these results also confirm the potential application of DEM data for flood submergence extraction and provide new ideas for the improvement of the subpixel mapping model. The proposed method can accurately generate water distribution maps in a practical and economical way.

INDEX TERMS DEM, pixel unmixing technology, subpixel mapping, water extraction.

I. INTRODUCTION

Water boundaries, which are the junctions where water and land meet, include lakeshores, river banks, coasts and flood boundaries. In water remote sensing applications, water boundaries and areas must be extracted, and the extraction accuracy will directly affect the accuracy of subsequent research. During water boundary extraction, the mixed pixel problem occurs. The influence of image spatial resolution on the result of water boundary extraction varies based on the area of the water body; the resolution may have little impact on a large water body, but it has a great impact on a small water body when using, for example, Landsat, Sentinel and other medium-resolution images [1]. When monitoring large water bodies (e.g., 100-ha lakes), medium-resolution

The associate editor coordinating the review of this manuscript and approving it for publication was Jenny Mahoney.

data such as Landsat and SPOT can be used to achieve highly precise results and errors as low as 1-2 % [2], [3]. SPOT (up to 2.5 m) is expensive and has a long revisit cycle (unless images are ordered). Landsat images are free and combining imagery from two Landsat satellites (e.g. aboard Landsat 8 and Landsat 7) can provide images every 8 days. Sentinel -2 (up to 10 m) (2A and 2B) can have a revisit time of 5 days, basically meeting the needs of flood monitoring. However, the rapid changes of the flood in a short period of time cannot be captured. Moreover, Sentinel-2 has only provided services in recent years and lacks historical reference data. In comparison, although the spatial resolution of MODIS images is low (250 or 500 m), it can obtain data every day, covering a wide range, with rich historical data since 2000. Therefore, MODIS images have broad application prospects in dynamic monitoring fields, such as flood monitoring, drought monitoring and marine environment monitoring. Most of

these applications require a wide range of coverage and high monitoring frequencies. [6], [7]. However, the low spatial resolution of MODIS images causes mixed pixels, which greatly limits the accuracy of MODIS water extraction and the application of MODIS in the field of water remote sensing. However, the need for unmixing methods is not limited to low spatial resolution imagery such as MODIS, as even with 10-m imagery, boundary error can be high on small water bodies. This method has potentially even greater benefits when studying small water bodies for which these border effects are more important.

Through pixel unmixing, the percentage of each feature among the mixed pixels (i.e., the end element abundance) can be obtained. However, to determine the specific spatial locations of the various types of features, the subpixel mapping algorithm is still required. In 1997, Professor Atkinson of the university of Southampton in the United Kingdom proposed the concept of subpixel mapping. For subpixel mapping, which is based on the theory of spatial correlation, the distributions of the feature category within and between pixels are assumed to be spatially correlated; therefore, pixels that are closer together are more likely to belong to the same type than pixels that are farther away [8].

Atkinson proposed a pixel swapping algorithm (PSA) based on the spatial correlation theory of pixels. Due to the correlation between a subpixel and its neighboring subpixels, subpixels can be exchanged to gradually increase the spatial correlation until stability is attained [9]. Ling Feng and others used cellular automata to exchange subpixels to maximize the spatial correlation [10]. Tatem proposed a subpixel mapping process for two types of features (i.e., target and background features) in combination with a Hopfield neural network (HNN) and then extended the model for the position determination of various target categories [11]. Subpixel mapping has been successfully applied in multiple remote sensing image applications [12], [13]. Kasetkasem *et al.* used Markov random fields (MRFs) to describe the statistical correlation between pixels by considering spatial and spectral constraints and realized subpixel mapping by calculating the probability of the various types of features belonging to subpixels [14]. Verhoeye *et al.* studied the mathematical model of the spatial correlation theory and transformed subpixel mapping into a linear optimization problem. On this basis, Mertens *et al.* proposed a genetic algorithm (based on the BP neural network (BPNN) [15], [16]) called the subpixel/pixel spatial attraction model (SPSAM) [17], [18]. For the SPSAM, according to spatial correlation theory, similar types of features are assumed to attract each other without prior information.

Although these algorithms are implemented differently, their basic principles are similar. For example, they are all based on the spatial correlations of feature information (i.e., the similarity principle), and they readily obtain compact figure shapes and are suitable for most types of figures. Subpixel mapping is an underdetermined inversion problem with constraints that are much less rigid than those of the

solution parameters, which leads to large uncertainties in the mapping results. Additional spatial distribution features describing the types of objects inside mixed pixels can be included. Auxiliary information, such as DEM elevation data, high-resolution remote sensing images, and feature boundaries, can be adopted as a constraint to improve the accuracy of subpixel mapping [19]–[21]. The distribution of water is closely related to the topography. Digital elevation model (DEM) data have been applied in many studies in combination with remote sensing image data for water distribution monitoring [7], [20].

Therefore, in this paper, a modified subpixel mapping algorithm is proposed. This method introduces DEM data and uses elevation values to determine whether a subpixel is a submerged pixel, thus, the traditional subpixel mapping is modified, and a higher accuracy for the submerged subpixel mapping of water bodies is achieved.

II. THEORY AND METHODS

Remote sensing image classification methods can be divided into two categories: hard classification methods and soft classification methods. Hard classification methods, which include supervised classification, unsupervised classification and decision tree classification, divide each pixel into a specific feature category, which will lead to the loss of a large amount of useful information and easily cause overestimation and omission. Soft classification methods calculate the percentage of a mixed pixel represented by each land type, obtain a rich image dependent on the number of ground classes, divide the mixed pixel into a plurality of subpixels, and determine each type of feature of the subpixel. Clearly, soft classification methods are scientific and reasonable, and they can optimally preserve useful image information.

A. END ELEMENT EXTRACTION

The endmember is a pure pixel that contains only one type of feature. Common algorithms for endmember spectral extraxtion include the pure pixel index (PPI), N-FINDR, and iterative error analysis (IEA) [22], [23]. The purity degree of end element selection has a great influence on the decomposition result of the mixed pixel. The PPI algorithm is the most mature and widely used approach, but it is sensitive to noise anomalies. There is no suitable selection rule for the intermediate process parameters, and the end element spectrum cannot be visually evaluated. The actual feature category is represented; thus, the accuracy of the algorithm in selecting the endmember is not guaranteed.

In view of the shortcomings of the PPI algorithm, this paper proposes a method that obtains the endmember directly from the MODIS image by using the high-resolution image surface coverage and PPI image as prior knowledge. Specifically, high- and low-resolution images acquired on the same day are almost the same in terms of surface coverage, and the PPI index indicates the pixel. We can first set the PPI index image to a higher threshold and then select the corresponding low spatial resolution based on the surface coverage of the

high-resolution remote sensing image. The spectrum of the corresponding position on the image is generated to obtain the endmember spectrum. This operation mode can intuitively control the type and quantity of the selected feature according to the actual object type, which greatly improves the efficiency and accuracy of endmember extraction.

B. ABUNDANCE INVERSION

The process of obtaining the end-element spectrum of the various types of features extracted from mixed pixels is called pixel unmixing. Existing pixel unmixing models mainly include linear and nonlinear models. Currently, the most widely used model is the linear spectral mixture model (LSMM). The LSMM assumes that the spectral features of a feature in a pixel are similar and exhibit linear additivity. The reflectivity of the pixel in a certain band is composed of pixels, and a linear combination of the end element reflectance is adopted as the weight factor of the pixel area ratio [23], [24].

C. SUBPIXEL MAPPING

Subpixel mapping is mainly based on the decomposition of mixed pixels, and it uses the feature types and their corresponding abundance values to cut the mixed pixels into smaller units, subdivide the units into subpixel levels, and determine the mixed pixels. The specific spatial location of the included feature types is used to obtain a subpixel-scale feature classification map to improve the spatial resolution of remote sensing feature images.

Based on Atkinson's theoretical research, Verhoeye *et al.* proposed a mathematical model that transforms the subpixel mapping problem into a subpixel distribution problem by using linear optimization. The model assumes that a large pixel is divided into S^2 small pixels, among which class c subpixels account for NSP_c. The numerical value of NSP_c is obtained from an abundance map. $SDV_{c,j}$ represents the spatial attraction of subpixel p_j when it is assigned to class c. When $x_{c,j}$ is equal to 1, subpixel p_j is of class c, and when $x_{c,j}$ is equal to 0, subpixel p_j is of a different class. The model can be expressed as follows:

$$\text{Maximize } Z$$
$$= \sum_c \sum_j x_{cj} \cdot SDV_{cj}, \tag{1}$$

$$x_{cj} = \begin{cases} 1, & \text{if subpixel } p_j \text{ is assigned to class } c, \\ 0, & \text{otherwise.} \end{cases} \tag{2}$$

The model has two constraints:

$$\sum_c x_{cj} = 1, \tag{3}$$

$$\sum_j x_{cj} = NSP_c. \tag{4}$$

Equation (3) indicates that subpixel p_j must be one of c types of ground objects, and equation (4) indicates that in a mixed pixel, the number of subpixels c should be equal to the

number of subpixels NSP_c determined by the decomposition of the mixed pixels [1].

The SPSAM is a simple and effective solution to the above spatial relation theory. The SPSAM is based on the following assumptions: First, the neighborhood pixels are spatially attracted to the subpixels in the central pixel, and gravity is determined based on the abundance and distance of the neighborhood pixels. Second, the subpixels in the central pixel are attracted by only the neighboring pixels (in general, there are eight such pixels). Third, other pixels are considered to be too far from the central pixel to produce attraction; a pixel near the center pixel is more attracted to the center pixel than the pixel far from the center pixel.
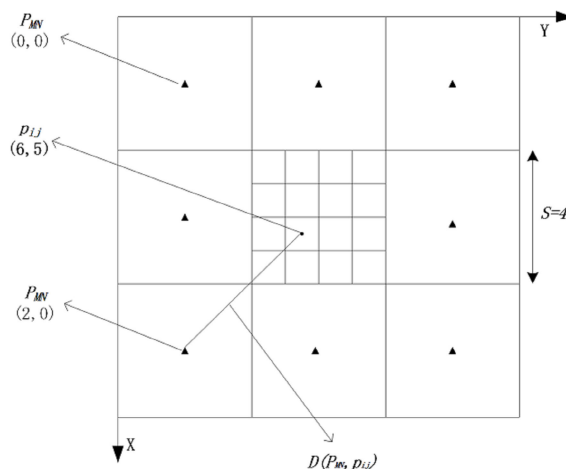

FIGURE 1. Illustration of the subpixel/pixel spatial attraction model (SPSAM) (adapted from [20]).

The SPSAM calculates the attraction based on the Euclidean distance. In the SPSAM, the correlation is described by the spatial attraction, and the category of each subpixel is determined by calculating the spatial attraction between each subpixel and its corresponding neighborhood. Figure 1 is a schematic diagram of the distance calculation of the SPSAM when the segmentation scale factor equals 4. The distance between subpixel Pij and neighboring pixel PMN in the central pixel can be expressed as:

$$d\left(P_{MN}, p_{ij}\right)$$
$$= \sqrt{[i + 0.5 - S(M + 0.5)]^2 + [j + 0.5 - S(N + 0.5)]^2},$$
$$(i, j = 0, 1, \ldots, 8; M, N = 0, 1, 2). \tag{5}$$

When subpixel p_{ij} is designated as class c, the spatial attraction of a neighboring pixel is expressed by $SDV_{c,j}$, and the equation is as follows:

$$SDV_{c,ij} = \sum_M \sum_N \frac{1}{d(P_{MN}, P_{ij})} F_c(P_{MN}), \tag{6}$$

where $F_c(P_{MN})$ is the abundance value of class c objects in the neighboring pixel P_{MN} [21]. The SPSAM algorithm, as a simple subpixel location method without prior information, has been widely used [18].

D. SUBPIXEL MAPPING CORRECTION

This paper attempts to introduce DEM elevation information to correct subpixel mapping errors. This method is referred to as the D-MSPSAM (DEM-Modified SPSAM), and it is written by Python. The basic idea of the algorithm is that the elevation of water is generally the lowest value of the pixel, and subpixels can be assigned to submerged pixels according to DEM elevation value. First, the number of water subpixels (n) in each pixel is obtained according to the abundance map (segment scale factor S^2 × water abundance). Then, n minimum values are taken from the corresponding DEM, which are regarded as the normal elevation range of water body, and each subpixel in the MODIS pixel is traversed. If the subpixel elevation is within the normal elevation range of the water, but the subpixel received a non-water classification, then the result is corrected to water; if the subpixel elevation is greater than the normal elevation range of the water, but the subpixel received a classification of water, then the classification is updated to reflect the species with the highest content. During this process, the water abundance is seen as a constraint (i.e., the number of subpixels is still n). This algorithm can greatly reduce underestimation and overestimation and thereby reflect the most reasonable distribution state of the water.

E. ACCURACY VERIFICATION

At this stage, there is no clear evaluation index to use to evaluate the subpixel mapping accuracy. However, since the result of subpixel mapping is usually the classification result, a traditional classification result evaluation index, such as the overall classification accuracy (OA), kappa coefficient, or confusion matrix, can be used to evaluate the subpixel mapping accuracy. The main flow chart of this work is shown in Figure 2.

III. EXPERIMENTS AND RESULTS

A. STUDY AREA OVERVIEW AND DATA SOURCES

Dongting Lake, which is the second largest freshwater lake in China, covering an area of 2625 km^2, is an important lake for sedimentation and storage in the Yangtze River Basin, and it maintains the ecological balance of rivers and lakes [25]. Water body distribution monitoring in the Dongting Lake area will provide a reference for flood risk management, disaster prevention and mitigation in the region and is of great significance for maintaining the safety in the middle and lower reaches of the Yangtze River.

The Moderate-resolution Imaging Spectroradiometer (MODIS) is mounted on Terra and Aqua satellites; Terra is a morning satellite, while Aqua is an afternoon satellite, and the two satellites cooperate to cover the entire surface of Earth every 1-2 days [26]. The MOD09GA/MYD09GA surface reflectance data are daily surface reflectance data that include 7 bands and are ideal remote sensing data for extracting flood submersion ranges. However, the spatial resolution of these data is 500 m, and the mixed pixel phenomenon
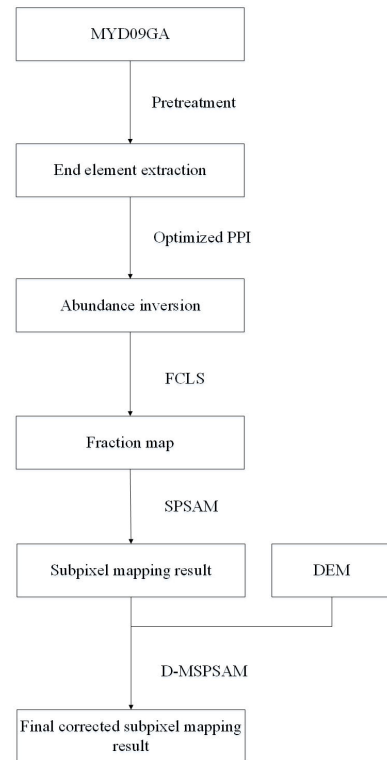

FIGURE 2. The main flowchart of this work.

is severe. Experiments with two MYD09GA images have been conducted for areas with high and low water [27]. Furthermore, two 30-m-resolution Landsat 8 Operational Land Imager (OLI) images acquired on the same day were selected as a reference for the water extraction results, and 30-m-resolution ASTGTM2 DEM data were selected as subpixel mapping auxiliary correction data [28]. SRTM (Shuttle Radar Topography Mission) and ASTER GDEM (Advanced Spaceborne Thermal Emission and Reflection Radiometer Global Digital Elevation Model) are currently two mainstream free DEM data. From the practical experience, the SRTM data is suitable for the study of large-scale areas with large terrain fluctuations. In comparison, ASTER GDEM is more suitable for the scale of the current study area [29]. So, in this article, we chose the second edition of ASTGTM2 published by ASTER GDEM in October 2011. The specific experimental data are summarized in Table 1.

TABLE 1. Description of the data used in this study.

Experiment	Image	Imaging time	Frame number
high water	MYD09GA	2017.10.30	h27v06
	Landsat 8 OLI	2017.10.30	123/40
low water	MYD09GA	2017.12.17	h27v06
	Landsat 8 OLI	2017.12.17	123/40

1) PRETREATMENT

In the pretreatment of the MYD09GA image, firstly, the MRT tool is used to re-project the corrected and calibrated image,
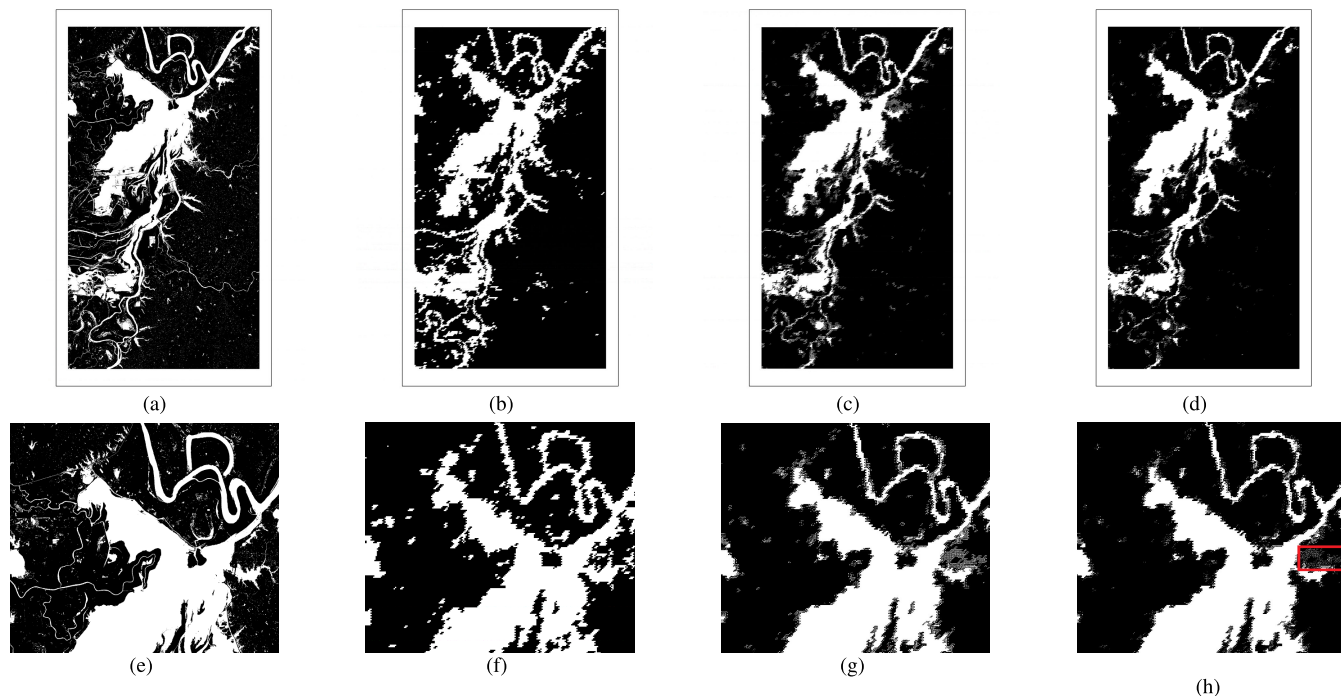
FIGURE 3. The result of the extraction of the flood submerged range under high water conditions. (a) Landsat reference image (31.25 m); (b–d) the results from MNDWI (250 m), SPSAM (31.25 m), and D-MSPSAM (31.25 m); (f-h) partially enlarged views of the results from the MNDWI, SPSAM, and D-MSPSAM.

and the projection was converted to UTM WGS84. Then, the image is resampled to 250 m by cubic convolution interpolation. Finally, the study area is obtained by cropping the image. Although the original pixel value is destroyed, compared with other methods, high-frequency information can be retained to the greatest extent, and noise can be smoothed. For Landsat images, radiometric calibration is first based on the MODTRAN5 radiation transmission model. Then, the Fast Line-of-sight Atmospheric Analysis of Hypercubes (FLAASH) model is used for atmospheric correction. Finally, the test area is cropped and resampled to 31.25 m. Here, the MODIS image resolution is an integer multiple of the Landsat image resolution (i.e., a MODIS pixel is divided into 8×8 subpixels). The MODIS image has the same resolution as the Landsat verification data after segmentation, and thus it can be accurately registered with MODIS data to facilitate superimposition analysis. Similarly, the DEM is resampled to 31.25 m at the same size as the subpixels after segmentation to modify the subpixel mapping results pixel by pixel.

2) MIXED PIXEL DECOMPOSITION
Based on the ground cover types in the study area, the end-element spectra of five ground cover types, including water, cultivated land, woodland, grassland, and bare soil, were extracted by using the end-element extraction method combined with the medium- to high-resolution images proposed in this paper. Then, the LSMM-based fully constrained least squares (FCLS) method is used to perform pixel unmixing and obtain the end-element abundance map and RMSE

image. The statistical RMSE frequency distribution revealed that RMS errors smaller than 0.020 accounted for more than 94 % in the two sets of experiments, which indicates that the end-element extraction algorithm proposed in this paper has a high accuracy and meets the subpixel mapping requirements.

3) SUBPIXEL MAPPING AND CORRECTION
Taking the end-element abundance map obtained from pixel unmixing as an input, the SPSAM algorithm is used to realize subpixel mapping of the flood submerged area. The subpixel mapping results are shown in Figure 3 (c). The result after adding DEM auxiliary information to modify Figure 3 (c) is shown in Figure 3 (d). Figure 3 (a) and Figure 3 (b) show the results of Landsat 8 and MODIS (500 m) extracted by the Normalized Difference Water Index (MNDWI) threshold method with 0 as the segmentation threshold [30]. To more intuitively compare the extraction effects of the algorithms, Figure 3 (a), (b), (c), and (d) are partially enlarged to obtain Figure 3 (e), (f), (g), and (h), respectively. The experiments considering the low water conditions were treated in the same way, and the results are shown in Figure 4.

4) ANALYSIS OF RESULTS
Comparing (a), (b), and (c) in Figures 3 and 4, it can be found that the subpixel mapping method and its modified results have clearer and more delicate water boundaries, thereby avoiding a large loss of detailed spatial information. Although the MNDWI threshold method can roughly extract the water range, the boundary is approximate, and the visual effect is
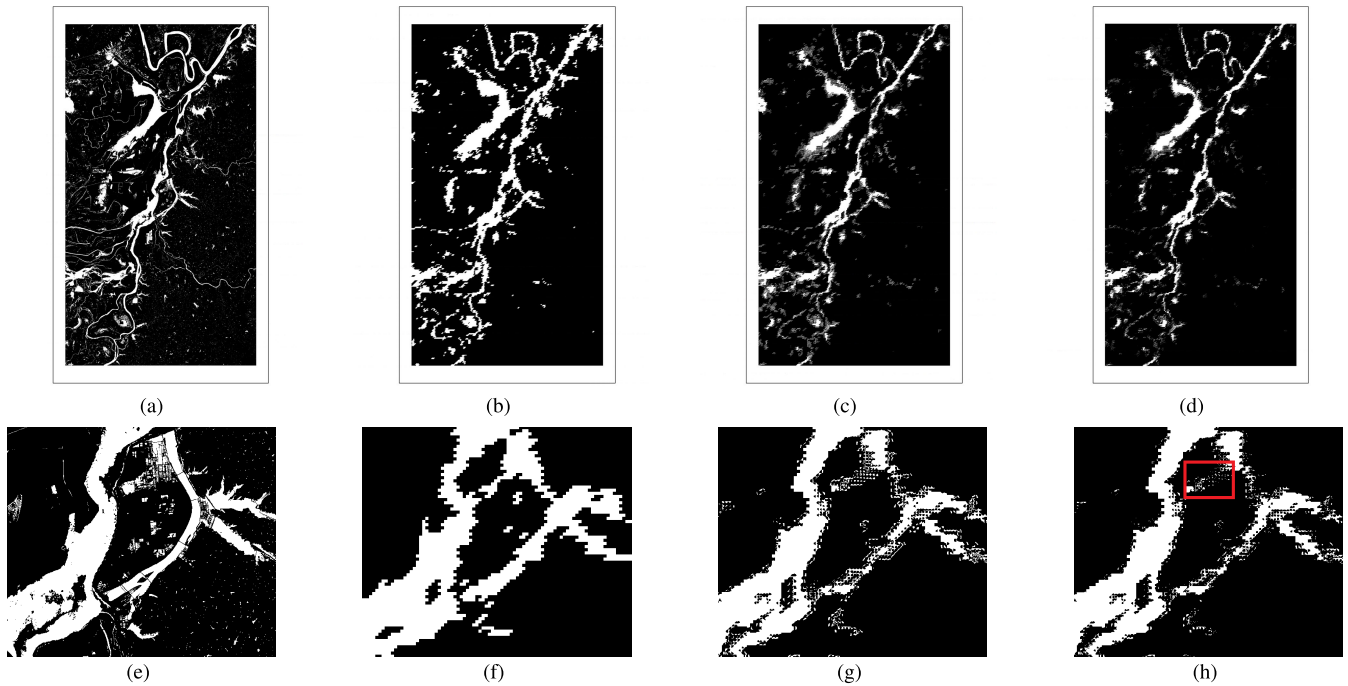
FIGURE 4. The result of extracting the flood submerged range under low water conditions. (a) Landsat reference image (31.25 m); (b–d) the results from MNDWI (250 m), SPSAM (31.25 m), and D-MSPSAM (31.25 m); (f-h) the partially enlarged views of the results from the MNDWI, SPSAM, and D-MSPSAM.

poor. The partially enlarged views (e), (f), and (g) show that both methods neglect some water bodies with widths of less than 5 MODIS pixels. This phenomenon occurs due to the lower spatial resolution of the MODIS image itself, which is unavoidable. Comparing (a), (c), and (d) in Figures 3 and 4, it can be found that, after the DEM correction of the subpixel mapping results, the water boundary is further corrected. The positions of the red boxes of (g) and (h) in Figures 3 and 4 can be compared, and in Figure (h), these areas are reclassified as non-aqueous bodies. Combined with the true color images, these areas correspond to cities and paddy fields, respectively. Because the spectral characteristics of cities and paddy fields are similar to those of water bodies, they will be classified as water bodies in (g). This classification is modified by addition of the height limitation condition of the position. The D-MSPSAM method can thus remove irrigated paddy fields from the classified image and more accurately distinguish areas where the flood propagates. Conversely, by excluding these irrigated fields, the D-MSPSAM method may be less suited when monitoring all areas under water, for instance in research on evapotranspiration and agriculture.

The experimental water extraction results were superimposed on the Landsat reference images, as shown in Figures 5 and 6. The figures clearly show the correctly classified, overestimated and underestimated points. Overestimated pixels are classified as submerged pixels in the extraction results but are nonsubmerged pixels in the Landsat reference image. Underestimated pixels are classified as nonsubmerged pixels in the extraction results but are submerged pixels in the Landsat reference image.

It can be seen from Figures 5 and 6 that all three measures can correctly extract the main lake area to meet the needs of basic flood monitoring, but there are also underestimation errors, mainly in the small tributaries and basins. The results of the MNDWI threshold method clearly show areas that are incorrectly segmented, mainly along linear water boundaries. However, in the subpixel mapping results, such errors have been significantly reduced. After DEM correction, overestimation phenomenon is further reduced.

Based on the accuracy evaluation chart, certain accuracy evaluation indexes can be calculated, such as the overestimation error, underestimation error, overall accuracy and kappa coefficient (see Table 2). By analyzing Table 2, the following conclusions can be drawn.

1. The D-MSPSAM has the highest overall accuracy, followed by the SPSAM, and the MNDWI threshold method has the lowest overall accuracy. Under high water conditions, the overall accuracy of the D-MSPSAM algorithm increased by 0.23 percentage points compared to that of the SPSAM and by 3.56 percentage points compared to that of the MNDWI. For the low water conditions, the overall accuracy of the D-MSPSAM algorithm is improved by 0.54 percentage points compared with that of the SPSAM and 2.77 percentage points compared with that of the MNDWI method. The kappa coefficient of the three methods also verifies this finding. The kappa values of the three results in the two experiments are all above 0.5, which indicates the experimental results are consistent with the Landsat reference images. DEM correction has the highest consistency, which shows it is the most consistent with the actual water distribution.
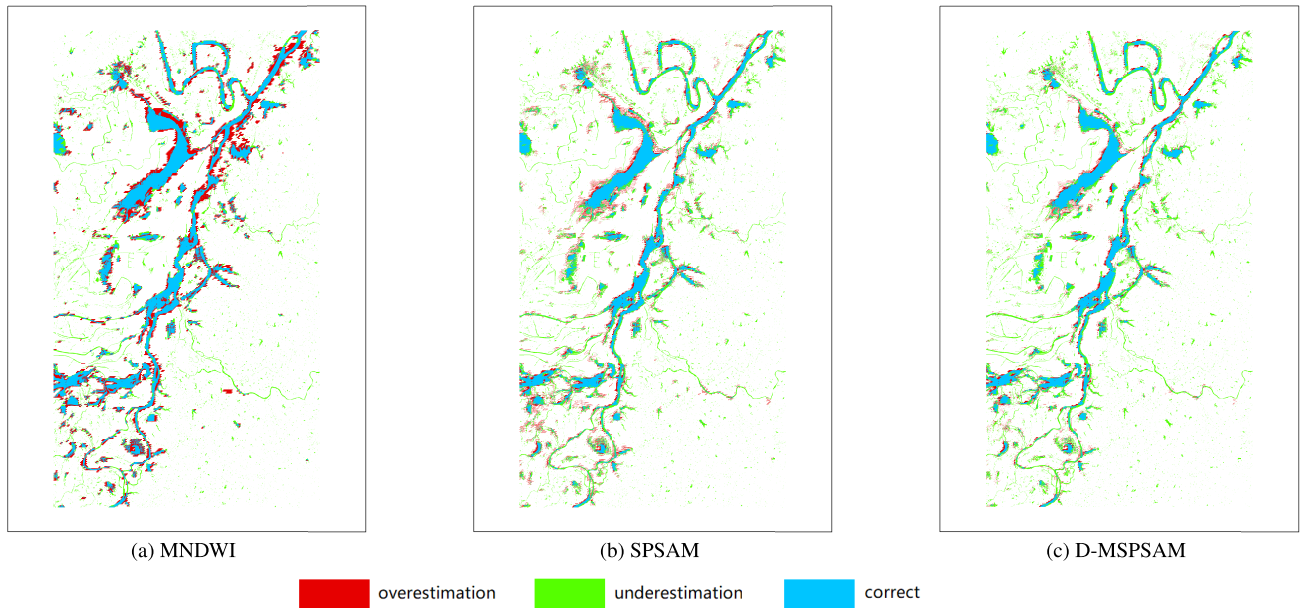
(a) MNDWI   (b) SPSAM   (c) D-MSPSAM

■ overestimation   ■ underestimation   ■ correct

FIGURE 5. Accuracy evaluation of water extraction results under high water conditions. (a–c) the accuracy evaluation results from MNDWI ((31.25 m), SPSAM (31.25 m), and D-MSPSAM (31.25 m).

TABLE 2. The accuracy evaluation indexes of the results.

Experiment	Method	Overall accuracy / %	Underestimation error / %	Overestimation error / %	Kappa coefficient
high water	MNDWI	87.84	6.52	5.63	0.65
	SPSAM	91.17	6.50	2.33	0.69
	D-MSPSAM	91.40	7.02	1.57	0.72
low water	MNDWI	89.70	5.21	5.10	0.53
	SPSAM	91.93	5.51	2.55	0.54
	D-MSPSAM	92.47	5.89	1.62	0.55

2. The MNDWI threshold method has the largest overestimation error, and the subpixel mapping error is reduced by more than half. Thus, the subpixel mapping method can effectively reduce overestimation and improve the precision of water boundary extraction. Furthermore, the overestimation error of the subpixel mapping results after DEM correction is further reduced to as low as approximately 1.6 %, and the extracted water boundary is more refined. In terms of the underestimation error, the three methods are not very different because they are limited by the lower spatial resolution of the MODIS data itself, and objects smaller than that resolution are not easy to identify.

3. The overall accuracy and kappa coefficient of the subpixel mapping results after DEM correction are further improved, the overestimation error is greatly reduced, and the underestimation error is slightly increased. The underestimation error slightly increases because of the Landsat reference image itself. Some regions with spectral information similar to water bodies, such as cities and urban areas, will be classified as water bodies. This is due to the modification of the correction algorithm by introducing elevation information.

In addition, the water to the right of the red rectangle in Figure 4 (h) is not very visible. Through observation, it is found that the main reasons for this phenomenon are as follows: First, on both sides of the river bank in the area, the elevation is close to that of the water body, which is difficult to correct due to the limitations of the D-MSPSAM algorithm. Second, there is a deviation in the registration of the DEM and MODIS images. Third, due to the image quality and extraction algorithm, there are abnormal values in the abundance extraction in this area. These underestimation problems must be addressed in future research. In summary, the experimental results demonstrate that the DEM corrects the subpixel mapping results, which verifies the application potential of the meta-location error and the effectiveness of the D-MSPSAM algorithm proposed in this paper.

4. The methods seem to work well for both the high and low water conditions. However, the results are better for the low water condition. We can see that the underestimation and overestimation errors at the low water condition are lower than those at the high water condition. The main reason for the low underestimation error under the low water condition

| (a) MNDWI | (b) SPSAM | (c) D-MSPSAM |

🟥 overestimation 🟩 underestimation 🟦 correct

FIGURE 6. Accuracy evaluation of water extraction results in low water conditions. (a–c) the accuracy evaluation results from MNDWI ((31.25 m), SPSAM (31.25 m), and D-MSPSAM (31.25 m).

TABLE 3. The accuracy evaluation indexes of the results in the test area.

Experiment	Method	Overall accuracy / %	Underestimation error / %	Overestimation error / %	Kappa coefficient
high water	MNDWI	89.40	5.59	5.02	0.76
	SPSAM	90.98	6.52	2.50	0.79
	D-MSPSAM	91.31	7.03	1.66	0.80
low water	MNDWI	88.33	3.51	8.16	0.67
	SPSAM	88.65	6.80	4.56	0.68
	D-MSPSAM	89.10	7.33	3.58	0.69

is that many small rivers are cut off or dried up, and the proportion of the total pixels is reduced. The low overestimation error during the low water condition is due to the small area and proportion of paddy fields and tidal flats, which are prone to overestimation. In addition, for the low water condition, the overall area of the water is small, and the areas of underestimation and overestimation are small. Thus, for small water bodies, subpixel mapping and correction algorithms can achieve good results.

The above discussion evaluates the accuracy of the whole image. The two areas of Figure 3 (e) and Figure 4 (e) in the two groups were selected as typical test areas for accuracy evaluation and effect analysis. Figure 3 (e) shows an urban area that contains large surface water bodies, linear water bodies, black surfaces and other non-aqueous bodies. Figure 4 (e) is a nonurban area that contains information on non-aqueous bodies such as small planar water bodies, small linear water bodies, and paddy fields. The accuracy evaluation results in Table 3 show that the overall accuracies of the D-MSPSAM in the two groups of experiments were 91.31 % and 89.10 %, which are better than those of the SPSAM and MNDWI threshold methods. In the high water condition, the overestimation error of the SPSAM and D-MSPSAM are reduced, and the overestimation error of

the D-MSPSAM is at least 1.66%. As this region contains cities and its spectral features are similar to water bodies, it is easy to be mistaken for water bodies in Landsat reference images, so its underestimation error is slightly higher than MNDWI threshold method. The rules of the SPSAM and D-MSPSAM corrected this issue. In the low water conditions, the underestimation errors of SPSAM and D-MSPSAM were significantly reduced. Compared with MNDWI threshold method, the overestimation error of D-MSPSAM decreased by 4.58 percentage points, and the underestimation error of D-MSPSAM increased by 3.82 percentage points, because the area contains rice fields. Furthermore, because the spectral characteristics of rice field are similar to those of water bodies, it is easy to mistakenly extract these areas as water bodies based on the Landsat reference image. The rules of the SPSAM and D-MSPSAM corrected this issue. In general, the accuracy verification results of the test area show the same trend as the overall accuracy verification results, and the conclusions are consistent. The subtle differences are related to the actual feature distribution in the area.

The experiment found that the extraction accuracy of the water body is mainly affected by two factors. The first factor is the type of water body in the study area. When the study area is dominated by planar water bodies, the classification

IEEE *Access*

accuracy is high (as shown in Figure 3 (e)); when the study area is dominated by small linear water bodies and there are few planar water bodies, due to the influence of mixed pixels, the classification accuracy will be low (Figure 4 (e)). The second factor is whether the area contains construction land and non-water body information such as mountain shadows, paddy fields or black surfaces.

IV. CONCLUSION AND DISCUSSION

Subpixel mapping technology can effectively enhance the spatial resolution of hyperspectral images and thereby improve the accuracy of target monitoring and recognition and promote the application of hyperspectral images in many fields. Therefore, it is of great significance to study subpixel mapping. Based on MOD09GA data, this paper uses the SPSAM algorithm to extract the water area of Dongting Lake. An improved D-MSPSAM subpixel localization algorithm has been proposed by adding elevation information to improve the positioning accuracy. The following conclusions can be drawn.

1. In this paper, the threshold method, subpixel mapping method, and improved subpixel mapping algorithm were used to perform water extraction experiments in the study area. The overall accuracy of the latter two methods are all above 91%, which exceeds the threshold method. Compared with the traditional hard classification water extraction methods, the subpixel mapping algorithm can improve the effective extraction of small water bodies and better maintain the spatial details of the water boundaries,and the overestimation error for the high water and low water conditions decreased by 4.06 percentage points and 3.48 percentage points, respectively.

2. Considering the close relationship between the DEM and water distribution, DEM elevation information was introduced to modify the subpixel mapping results. The experiment have proved that the accuracy of the subpixel mapping results after the DEM correction were further improved, which has provided a new idea for the improvement of the subpixel mapping model. The method proposed in this paper can be applied to many fields such as surface cover extraction, coastal zone extraction, and change monitoring. However, due to the low spatial resolution and complex ground spectral information, the subpixel mapping results still show overestimation and underestimation errors. In addition to continuously improving the algorithms to improve the mapping accuracy, various auxiliary information can be introduced to modify the subpixel mapping results.

Based on the research results of this article, the following issues need to be further studied:

1. End-element extraction, pixel unmixing, and subpixel mapping are closely related. In the application process, end-element extraction, mixed pixel decomposition, and finally subpixel mapping are sequentially performed. Previous results are used as inputs for the next step, and the inputs can have a very large impact on the final result. Therefore, the previous link cannot be disconnected from the subsequent step, and it is thus necessary to build a comprehensive mixed

pixel analysis model. A suitable and comprehensive analytical model with universal applicability is needed.

2. The spatial distribution of features is the focus of subpixel mapping. Although many methods describe such distributions, such as the theory of spatial correlation maximization, these methods all have shortcomings. Thus, a more effective description of the correlations among complex objects is still needed.

3. This paper validates the improved subpixel mapping method by adding the DEM elevation information through two sets of experiments. Different terrain distributions will have a certain impact on the performance of the algorithm. For hyperspectral images of different regions, the influence of the terrain distribution on the mapping accuracy must be reduced. In addition, since satellite-based DEM has some problems in gap correction and vegetation correction, the results are uncertain. Therefore, in subsequent research, we will try other types of DEMs (e.g., merit DEM, Tandem-X DEM) to improve the accuracy of the D-MSPSAM.

REFERENCES

[1] F. Ling, S. Wu, and F. Xiao, "Sub-pixel mapping of remotely sensed imagery: A review," *J. Image Graph.*, vol. 16, no. 8, pp. 15–64, 2011.
[2] R. Díaz-Delgado, D. Aragonés, I. Afán, and J. Bustamante, "Long-term monitoring of the flooding regime and hydroperiod of Doñana marshes with Landsat time series (1974–2014)," *Remote Sens.*, vol. 8, no. 9, pp. 123–135, 1993.
[3] H. Bi, S. Wang, J. Zeng, Y. Zhao, H. Wang, and H. Yin, "Comparison and analysis of several common water extraction methods based on TM image," *Remote Sens.*, vol. 27, no. 5, pp. 77–82, 2012.
[4] C. Leauthaud, G. Belaud, S. Duvail, R. Moussa, O. Grünberger, and J. Albergel, "Characterizing floods in the poorly gauged wetlands of the Tana river delta, Kenya, using a water balance model and satellite data," *Hydrol. Earth Syst. Sci.*, vol. 17, no. 8, pp. 3059–3075, Aug. 2013.
[5] A. Ogilvie, G. Belaud, C. Delenne, J.-S. Bailly, J.-C. Bader, A. Oleksiak, L. Ferry, and D. Martin, "Decadal monitoring of the Niger inner delta flood dynamics using MODIS optical data," *J. Hydrol.*, vol. 523, pp. 368–383, Apr. 2015.
[6] Y. Chen, C. Huang, C. Ticehurst, L. Merrin, and P. Thew, "An evaluation of MODIS daily and 8-day composite products for floodplain and wetland inundation mapping," *Wetlands*, vol. 33, no. 5, pp. 823–835, Oct. 2013.
[7] C. Huang, Y. Chen, and J. Wu, "DEM-based modification of pixel-swapping algorithm for enhancing floodplain inundation mapping," *Int. J. Remote Sens.*, vol. 35, no. 1, pp. 365–381, Jan. 2014.
[8] P. M. Atkinson, "Mapping subpixel boundaries from remotely sensed images," in *Proc. Innov. GISs*, vol. 4, 1997, pp. 166–180.
[9] P. M. Atkinson, "Sub-pixel target mapping from soft-classified, remotely sensed imagery," *Photogramm. Eng. Remote Sens.*, vol. 71, no. 7, pp. 839–846, Jul. 2005.
[10] F. Ling, Q.-W. Zhang, C. Wang, and J.-Z. Zhou, "Sub-pixel mapping of remote sensing images based on cellular automata model," *J. Image Graph.*, vol. 10, no. 7, 2005, pp. 916–921.
[11] A. J. Tatem, H. G. Lewis, P. M. Atkinson, and M. S. Nixon, "Super-resolution target identification from remotely sensed images using a Hopfield neural network," *IEEE Trans. Geosci. Remote Sens.*, vol. 39, no. 4, pp. 781–796, Apr. 2001.
[12] A. Tatem, "Super-resolution land cover pattern prediction using a Hopfield neural network," *Remote Sens. Environ.*, vol. 79, no. 1, pp. 1–14, Jan. 2002.
[13] A. J. Tatem, H. G. Lewis, P. M. Atkinson, and M. S. Nixon, "Increasing the spatial resolution of agricultural land cover maps using a Hopfield neural network," *Int. J. Geographical Inf. Sci.*, vol. 17, no. 7, pp. 647–672, Oct. 2003.
[14] T. Kasetkasem, M. Arora, and P. Varshney, "Super-resolution land cover mapping using a Markov random field based approach," *Remote Sens. Environ.*, vol. 96, nos. 3–4, pp. 302–314, Jun. 2005.

[15] K. C. Mertens, L. Verbeke, and R. D. Wulf, "Sub-pixel mapping with neural networks: Real-world spatial configurations learned from artificial shapes," in *Proc. 4th Int. Symp. Remote Sens. Urban Areas*, 2003, pp. 117–121.

[16] K. Mertens, "Sub-pixel mapping and sub-pixel sharpening using neural network predicted wavelet coefficients," *Remote Sens. Environ.*, vol. 91, no. 2, pp. 225–236, May 2004.

[17] K. C. Mertens, B. De Baets, L. P. C. Verbeke, and R. R. De Wulf, "A sub-pixel mapping algorithm based on sub-pixel/pixel spatial attraction models," *Int. J. Remote Sens.*, vol. 27, nol.15, pp. 3293–3310, Sep. 2006.

[18] L. Lu, Y. Huang, L. Di, and D. Hang, "A new spatial attraction model for improving subpixel land cover classification," *Remote Sens.*, vol. 9, no. 4, 2017, pp. 360–375.

[19] L. Giustarini, M. Chini, R. Hostache, F. Pappenberger, and P. Matgen, "Flood hazard mapping combining hydrodynamic modeling and multi annual remote sensing data," *Remote Sens.*, vol. 7, no. 10, pp. 14200–14226, Oct. 2015.

[20] J. M. Karlsson and W. Arnberg, "Quality analysis of SRTM and HYDRO1K: A case study of flood inundation in mozambique," *Int. J. Remote Sens.*, vol. 32, no. 1, pp. 267–285, Jan. 2011.

[21] J. D. G. Osorio and S. G. G. Galiano, "Development of a sub-pixel analysis method applied to dynamic monitoring of floods," *Int. J. Remote Sens.*, vol. 33, no. 7, pp. 2277–2295, Apr. 2012.

[22] A. Song, A. Chang, J. Choi, S. Choi, and Y. Kim, "Automatic extraction of optimal endmembers from airborne hyperspectral imagery using iterative error analysis (IEA) and spectral discrimination measurements," *Sensors*, vol. 15, no. 2, pp. 2593–2613, Jan. 2015.

[23] W. Xiong, C.-I. Chang, C.-C. Wu, K. Kalpakis, and H. M. Chen, "Fast algorithms to implement N-FINDR for hyperspectral endmember extraction," *IEEE J. Sel. Topics Appl. Earth Observ. Remote Sens.*, vol. 4, no. 3, pp. 545–564, Sep. 2011.

[24] A. Plaza, G. Martín, J. Plaza, M. Zortea, and S. Sánchez, "Recent developments in endmember extraction and spectral unmixing," in *Proc. Opt. Remote Sens.*, 2011, pp. 235–267.

[25] Z. Zhang, X. Li, and Y. Zheng, "Research on flood storage function and change law of Dongting Lake," *J. Sediment Res.*, no. 2, pp. 68–74, Apr. 2014.

[26] C. Leauthaud, S. Duvail, G. Belaud, J. Albergel, R. Moussa, and O. Grunberger, "Contribution of MODIS satellite imagery in modelling the flooding patterns of the coastal wetlands of the Tana River, Kenya," in *Proc. EGU Gen. Assem. Conf. Abstr.*, vol. 14, 2012, p. 10514.

[27] *NASA Official Website*. [Online]. Available: http://reverb.echo.nasa.gov/reverb/

[28] *USGS Official Website*. [Online]. Available: http://earthexplore.usgs.gov/

[29] Y. Liu, M. Zhang, and Y. Li, "Contrastive analysison two external free DEM data," *Sci-Tech Innov. Productiv.*, no. 6, pp. 73–75, Jun. 2014.

[30] H.-Q. Xu, "A study on information extraction of water body with the modified normalized difference water index (MNDWI)," *J. Remote Sens.*, vol. 9, no. 5, pp. 589–595, Sep. 2005.

NA ZHANG received the B.S. and M.S. degrees from the Shandong University of science and Technology, Qingdao, China, in 2016 and 2019, respectively. Her research interest includes application of remote sensing technology.

PING WANG received the B.S., M.S., and Ph.D. degrees from the Shandong University of Science and Technology, Qingdao, China, in 1987, 1994, and 2004, respectively. She is currently a Professor and a Ph.D. Tutor of remote sensing with the Shandong University of Science and Technology. Her research interest includes monitoring of ecological environment of resources.

XIN ZHAO received the B.S. degree from Shandong Agriculture Engineering University, Jinan, China, in 2017, and the M.S. degree from the College of Geomatics, Shandong University of Science and Technology, Qingdao, China, in 2020, where she is currently pursuing the Ph.D. degree. Her current research interests include remote sensing of resources and environment and image registration.

● ● ●